Design Procedure and Testing for the Electrification of a Maintenance Railway Vehicle

Davide D'Amato [1,*,†], Marco Lorito [2,†], Vito Giuseppe Monopoli [1,*,†] , Rinaldo Consoletti [1,†], Giuseppe Maiellaro [2,†] and Francesco Cupertino [1,†]

1   Department of Electrical and Information Engineering, Politecnico di Bari, Via E. Orabona, 4, 70125 Bari, Italy
2   Tesmec Rail Srl, Via A. Fogazzaro, 51, 70043 Monopoli, Italy
*   Correspondence: davide.damato@poliba.it (D.D.); vitogiuseppe.monopoli@poliba.it (V.G.M.)
†   These authors contributed equally to this work.

Abstract: In response to climate change, governments around the world have committed to reducing greenhouse gas emissions, which contribute to global warming, through the energy transition from fossil fuels to renewable energy sources and electrification of transportation. This article outlines the design procedure for the electrification of a railway vehicle used for maintenance services on the rail network. The proposed methodology consists of the design of both an all-electric propulsion system and storage system with the aim of zero emissions when the vehicle is operating in tunnels and to minimise noise during maintenance services in cities. After highlighting the characteristics of the railway vehicle under consideration, a simulation model of the propulsion and generation system was developed in order to calculate the energy consumption of the entire railway system. Finally, experimental tests carried out on the prototype proved the effectiveness of the design procedure adopted and the proposed mathematical model, showing a good matching with the simulated results.

Keywords: energy storage design; lithium battery; all-electric propulsion system; railway

1. Introduction

The transportation sector is one of the main contributors to the increase in greenhouse gas (GHG) emissions, as it accounts for 25% of all CO_2 emissions in Europe [1]. Therefore, the electrification of transport is one of the objectives defined in various international treaties for the reduction of CO_2 and the integration of renewable energy sources [2–5]. The railway sector is considered to be the most environmentally friendly considering that the ratio of emissions to passengers transported is very low compared to other vehicles. However, it is responsible for 4.2% (336 million tCO_2) of the CO_2 emissions produced by global transport [1]. In order to achieve zero emissions by 2050 [3], the electrification of new railway lines, electricity generation through the use of renewable sources, and the development of high-speed trains are being developed.

Recently, high-speed trains have become a viable alternative to international flights due to the development of new railway lines connecting several countries. These high-speed trains intended to travel long distances have the pantagraph–catenary interaction to feed the on-board loads as is already present for conventional trains. The catenary is an overhead line system installed along the entire railway line, and through its contact with the pantograph installed on the roof of the train, it supplies the electrical current required to power the electric motor and loads [6]. However, the catenary is subject to continuous impact with the pantograph and is exposed to environmental loads, thus representing one of the most-vulnerable elements of the railway system, a source of failures and increased maintenance costs [7,8]. In addition, many countries still have non-electrified railway networks [9], and the investment and operating costs for the creation of new electric railway networks are high, so catenary-free electric trains have become one of the newest technologies for rail transport, whose power is supplied through storage systems.

Consequently, it is essential to search for cleaner propulsion alternatives and to develop on-board energy storage devices [10].

In this context, several public transport companies in Italy, as in other countries in Europe and around the world, have carried out various projects and are investing in solutions for environmentally friendly traction systems and integrating low-polluting technologies such as lithium-ion batteries [11–13] and fuel cells [14–16]. An example is the project proposed in [12], presenting one of the first battery-powered trains to enter passenger service in Europe. The storage system is designed to provide a range of 100 Km on non-electrified railway lines and travel at a speed of 140 Km/h with a maximum acceleration of 1.1 m/s^2. The battery pack is lithium-ion and has the ability to support fast research, allowing recharging in 7–10 min.

There are several projects and studies in the literature presenting the electrification of railway vehicles used for non-electrified lines and railway vehicles in which the storage system is the main power source.

In these studies, the design procedure of the storage system is mainly based on optimisation problems [17,18] or approaches based on mathematical modelling in simulation [19,20]. The paper presented in [17] highlights the key points for the dimensioning of the storage system for a passenger train, a metro, and an urban tram, all of which are not connected to the catenary. The design of the battery was carried out through an optimisation problem considering the energy and power required by the three trains along the route under consideration.

Numerical simulation in the MATLAB/Simulink environment is a widely used methodology for designing a storage system and calculating the energy consumption of the battery, as is proposed in the work in [19], where an Electric Multiple Unit (EMU) was designed with the intention of installing it on the new electric trains to replace the conventional diesel trains, thus reducing emissions. The battery and the entire integration system were modelled in a simulation, and the energy consumption of the battery was calculated. The authors claimed that the new electric solution is able to reduce fuel costs and carbon dioxide emissions by 86.67% and 64.96%, respectively, for a 12 Km stretch from Ubungo-Maziwa to the city centre of Dar es Salam, Tanzania.

Mathematical modelling allows evaluating several technical solutions and choosing the optimal ones based on the characteristics of the designed system, as proposed in the work [20], where four different configurations based on combinations of fuel cells and/or batteries were compared on a real passenger train tested on a line from Catanzaro Lido to Reggio Calabria, Italy. Through simulation results, fuel cell efficiency, hydrogen consumption, battery state of charge (SOC), and energy recovery during braking were compared in order to determine the most-viable configuration. These studies show how a design procedure based on mathematical modelling in simulation can reduce development time and simplify the identification of design errors, as well as being an easy tool that can provide results close to the "real case". However, few works are available in the literature that describe the design process of both the propulsion and generation systems for a railway vehicle; the majority of studies focus on the sizing of a single component, such as electric motors for propulsion or energy generation systems [17–24].

With this in mind and considering the aspects discussed above, the main contribution of this article is to present the methodology and design procedure that were performed for the dimensioning and realisation of both of the entire all-electric propulsion system and the lithium-ion storage system of the rail vehicle under investigation. The design procedure, summarised in Figure 1, was based on the implementation in MATLAB/Simulink of the mathematical model of the entire railway system from which the technical solutions of the storage system and the propulsion system can be simulated. The proposed model was able to estimate the energy consumption of the entire storage system and the power that the propulsion system would have to provide to ensure the proper operation of the train. Through the simulation results, it was possible to size the electric motor, converters, battery, and braking resistor. Subsequently, after developing the prototype, experimental tests were carried out to validate the design choices and methodology performed. The design

choices that were made for sizing and component selection will be described, providing the reader with guidelines on the design of the entire power train. The design procedure was applied to a Tesmec Rail railway vehicle. This vehicle is used for the maintenance of the railway network; it operates in tunnels and urban centres, where it is necessary to perform low-emission work and minimise noise during maintenance services in urban centres.

The remainder of the paper is organised as follows. Section 2 presents a description of the railway vehicle under consideration. Section 3 implements the mathematical model of the entire railway system from the mathematical equations representing the individual components. Section 4 describes the criteria adopted for the design of the components. Section 5 shows the results of the simulation and experimental tests. Concluding remarks and future initiatives are presented in Section 6.
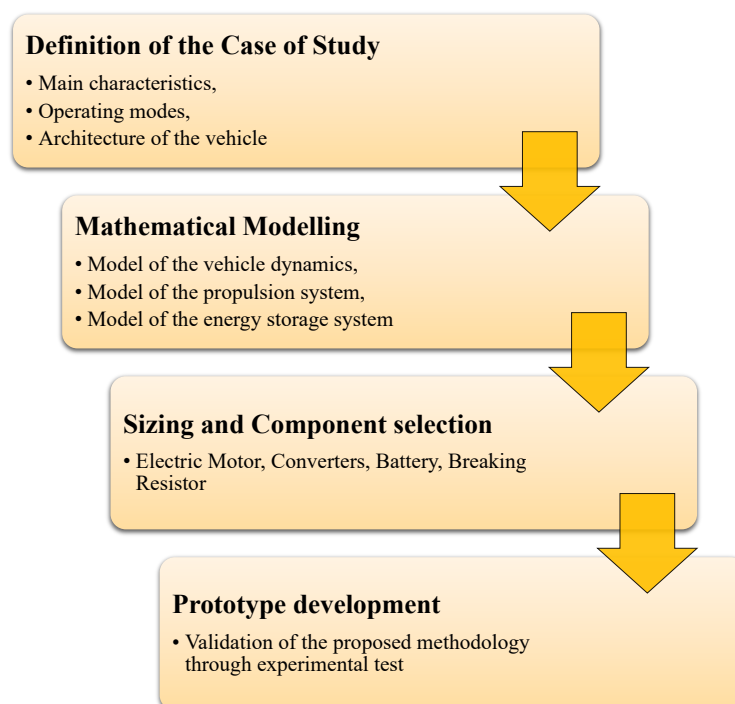
Definition of the Case of Study

- Main characteristics,
- Operating modes,
- Architecture of the vehicle

Mathematical Modelling

- Model of the vehicle dynamics,
- Model of the propulsion system,
- Model of the energy storage system

Sizing and Component selection

- Electric Motor, Converters, Battery, Breaking Resistor

Prototype development

- Validation of the proposed methodology through experimental test

Figure 1. A general overview of the methodology and design procedure for the electrification of a maintenance railway vehicle.

2. Case of Study

The APLA100-E is a railway vehicle used in the vicinity of cities or tunnels, where it is necessary to use environmentally friendly solutions and minimise noise during maintenance services. The APLA100-E, being a diagnostic vehicle, consists of working equipment such as a crane and a work platform, as can be seen in Figure 2. The main technical characteristics of the vehicle are summarised in Table 1.

The vehicle's electrical system is bimodal with two main sources of energy, the diesel generator and the lithium-ion battery storage system. The first is used for emergencies, i.e., only in the event of a breakdown or battery recharge. Indeed, the storage system is designed to fully meet the energy required during vehicle operation. In emergency mode, when the diesel generator is in operation, an AC/DC converter is interposed to convert the 380 VAC voltage to the DC bus voltage. As can be seen in Figure 3, the DC bus voltage is generated directly from the battery. There is no interface DC/DC converter between the battery and the power grid, in order to reduce the weight and bulk of the power system and the conversion losses during battery charging and discharging, a solution that has recently been used in several projects for light vehicles and small ships [25]. Furthermore, a lithium-ion battery was chose whose voltage variation with respect to the state of charge is small, as illustrated in Section 4. A pre-charge circuit was implemented to interface the

storage system to the grid. The pre-charge circuit is essential to avoid damaging the power source when it is connected to the grid, because when the battery is connected to a load with a capacitive input, such as the intermediate circuit of the inverter used for traction, an overcurrent occurs, known as the "inrush current", in the first few moments, both during startup and during commissioning. If this overcurrent is not limited, it can cause serious damage to system components. When the vehicle brakes during the duty cycle, the electric traction motor functions as a generator; the generated current can be used to charge the battery or be dissipated if the storage system is already fully charged.
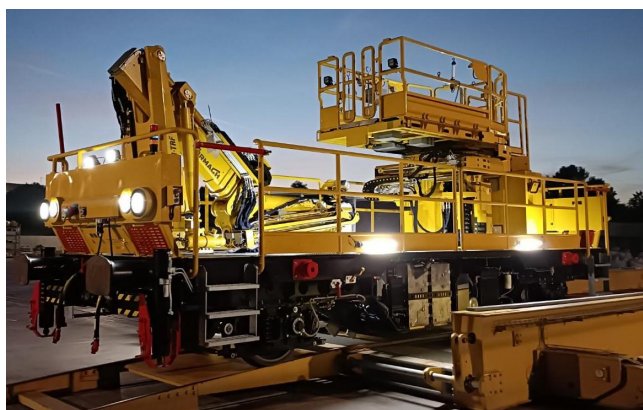

Figure 2. APLA100-E vehicle.

Table 1. Main characteristics of the APLA100-E vehicle.

Parameter	Value	Unit
Track gauge	1.435	m
Max length (between headstocks)	9.00	m
Max width	3.00	m
Overall length (including couplers)	10.240	m
Max height	3.450	m
Wheelbase	6.000	m
Max weight per axle	16	T
Max speed in convoy (towed)	100	km/h
Max speed in working mode	9	km/h

A braking resistor is sized to dissipate the excess current generated by braking or descending. However, it must be considered that the APLA100-E vehicle is relatively light and its duty cycle involves small movements with consequent braking of short a duration, as we shall see in the next sections. The amount of current generated can, therefore, be considered minimal, and the sizing of the braking resistor does not entail any critical issues in terms of weight and overall dimensions. The auxiliary power supply consists of a battery system necessary to power the 24 V circuit of the vehicle and the starting circuit of the diesel generator, and a DC/AC converter is also provided for the supply of AC sockets for any tools to be used during work operations. The movement of the crane and mobile terrace machinery is achieved by means of hydraulic circuits.
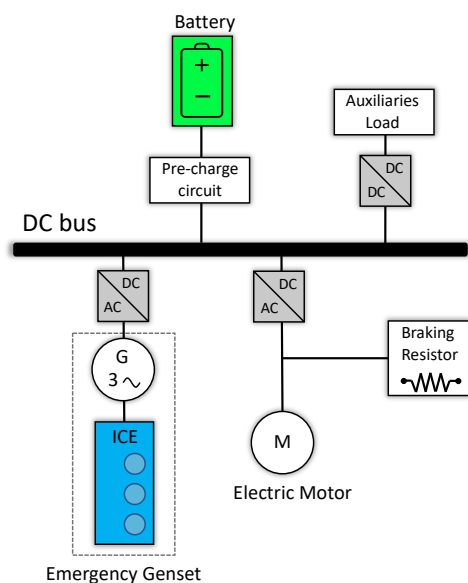
Figure 3. Architecture of the designed electrical system.

3. Mathematical Modelling

Following the establishment of the main characteristics of the vehicle and electrical system, the next step is modelling the entire railway system in a simulation. In this paper, the aim of the simulation was to model the dynamics of the vehicle, the entire propulsion system, and the storage system in order to obtain an estimate of the energy consumption of the railway system required for the sizing of the entire power train. The proposed design procedure consisted of identifying the optimal technical solutions for the electric motor, inverter, battery, DC/DC converter, and braking resistor. This is different from the work proposed in [23,24], where a simulation model was developed only for the generation system. The software used to develop the simulation models was MATLAB/Simulink because it allows the entire railway system to be implemented in a very simple and intuitive manner using a block diagram language. The dynamics of the various components were implemented through subsystems so that they can be easily modified and replaced. In addition, the implemented simulation provided acceptable results, as described in Section 5. In addition, the developed model allows even very long work cycles to be simulated in a few seconds.

The study of the electrical power required by the vehicle can be conducted by adopting different analysis methods [26,27]; two different simulation approaches can be distinguished according to the "direction" of the calculation method adopted: forward or backward. In a forward simulation approach, there is a control block that sends control actions such as acceleration or braking commands to the different components of the system to follow the desired speed of the vehicle. The driving model will then modify its command according to the proximity of the track. In contrast, in the backward method [23,28], the controller is not present and the analysis is made starting from the desired driving cycle of the vehicle, i.e., the time evolution of the vehicle speed. The value of the desired speed is transferred from the vehicle's dynamic model to the transmission and the motor in order to analyse the performance of the components and to derive the required power for the power system.

In this work, the model was based on the forward approach, as can be seen from the diagram in Figure 4. Indeed, an integral proportional speed control was implemented in order to reduce the difference between the actual speed of the vehicle and the reference profile. From the output of the control block comes the command that influences the operation of the electric motor, which then receives the torque reference from the motor.

The total torque transmitted by the motor has both a driving torque component, during the pulling phase, and a braking component when regenerative electric braking is desired. In addition, isoefficiency curves were implemented for both the electric motor and the control inverter to take into account the internal power losses that need to be considered when performing an energy analysis of the drive system. Therefore, using the overall efficiency of the drive system at various values of torque and rotational speed, it is possible to derive the electrical power required to power the system from the mechanical power required at the axis. This electrical power will be drawn from the storage system. By varying the voltage at the ends of the accumulator system, it is possible to know the electric current required to power the system and provide the desired torque. The model of the storage system incorporates the value of the current to know the discharged capacity and estimate its state of charge. The vehicle model essentially represents the longitudinal dynamics model of the vehicle, as it implements the resistances to motion present when the vehicle moves with a given velocity profile [29].

All the details of the model briefly discussed will be explained in depth in the following subsections, describing the methods and analyses required to develop the single blocks and then implement the complete model.
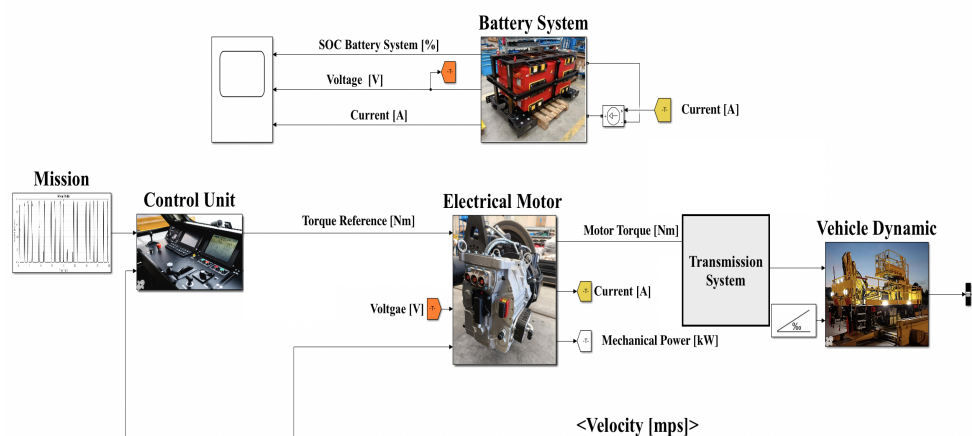

Figure 4. Block diagram of the implemented forward model.

3.1. Mission Profile

The operations of the vehicle are typical of rail maintenance vehicles, and therefore, it is mainly used for all work required for the construction and/or maintenance of the railway power line such as the laying of feeders and the installation of earth conductors. The maximum traction speed is 9 Km/h, and the duty cycle of the vehicle was assumed to last 2 h per 8-h turn. All the various activities that the vehicle is called on to carry out during its duty cycle can be expressed through the following Table 2.

Table 2. APLA100-E working cycle scenarios.

Type of Operation	Number of Operation	Duration
Traction start	30	-
Traction work	30	30 min
Traction stop	30	-
Equipment movement	60	40 min
Stopping for work execution	25	50 min

In order to design the entire storage system and also the vehicle's electrical system, several simulations were carried out assuming different gradients of 10‰, 35‰, −10‰ and −35‰. The tabulated data for the starting, traction, and stopping phases allowed a power profile of the vehicle to be derived, as shown in Figure 5. After deducting the time required for the start-up and stopping transients, which depend on the slope conditions of the

section on which the vehicle is to operate, a total of two hours of work was developed. The vehicle's storage system is capable of powering both the traction system and the machinery-handling system.
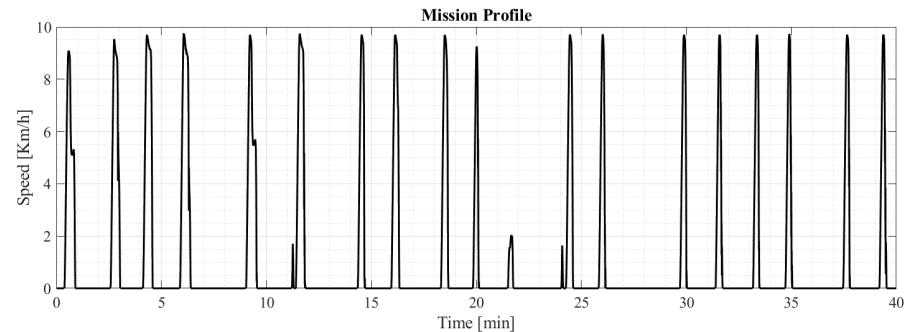

Figure 5. The mission profile of railway vehicle during the forty-minute work cycle.

3.2. Vehicle Dynamic

In order to analyse vehicle performance, it is necessary to create a model of the machine that is able to represent the dynamics to which the vehicle is subject when it is in motion. In the literature, there are different types of train models with more or fewer degrees of freedom (DOFs) [30]. The 2D and 3D train models with more degrees of freedom are used to perform simulations where both longitudinal and transverse dynamics need to be considered; these models, even if they produce accurate results, are complicated to implement and have a high computational cost. In this work, it was chosen to model the train as a rigid body with only one degree of freedom so that only longitudinal dynamics can be represented, neglecting transverse dynamics [29,31]. The equation of longitudinal dynamics takes into consideration the acceleration to which the vehicle is subjected, which has a certain mass, which is given by the difference between the traction effort and the resistance to motion. Tractive effort is the force capable of moving the vehicle with a certain speed when there is a certain resistance to motion. The mathematical relationship governing the longitudinal motion of the vehicle is provided by the main equation of the dynamic equilibrium, as follows:

$$F - R_{tot} = M_{ass} * a \tag{1}$$

where a is the acceleration of the train, while M_{ass} is the equivalent mass of the vehicle. The resistance R_{tot} of the train is related to the sum of the forces acting on the wheel against the motion of the vehicle. The resistance forces reduce the effect of the forces created by the propulsion devices, thus reducing the speed of the train. In this paper, both rolling resistance R_r and aerodynamic resistance R_a were considered, which depend exclusively on the vehicle's construction characteristics, and the additional resistances, which depend on the characteristics of the road such as the gradient resistance R_g.

$$R_{tot} = R_r + R_a + R_g \tag{2}$$

Having defined the resistances, it is possible to derive the acceleration through Equation (1), which can be rewritten in expression Equation (3).

$$\frac{dv}{dt} = \frac{F - R_r + R_g + R_a}{M_{ass}} \tag{3}$$

Integrating this equation yields the value of the vehicle's actual speed relative to the reference value, through which the motor torque can be adjusted. Furthermore, it is possible to calculate the rotational speed of the wheel and the torque required to make the vehicle move and, thus, overcome the resistive torque.

3.3. Electric Drive Model

To create the electric motor model, the mechanical characteristics of the motor, i.e., the angular torque–velocity curve, were taken into account. The study conducted was an energy analysis, and therefore, it was sufficient to assess the overall efficiency of the electric drive. In order to do this, the efficiencies of the inverter and motor were considered, which made it possible to determine the power absorbed and, consequently, the power supplied by the batteries. The electrical machine was subject to various types of losses during its operation, both losses in the conductors that make up the windings, typically copper, and losses in the iron and mechanical losses, due to friction and ventilation, which must be taken into due account. Through the calculation of internal motor losses, it is possible to trace the electrical power supplied to the input of the electric motor by knowing the mechanical power supplied to the shaft P_d. The electrical power is then related to the efficiency η_{EM} of the motor by the following relationship:

$$P_{EM} = \frac{P_d}{\eta_{EM}} \tag{4}$$

The behaviour of the electric motor can be effectively described by means of the mechanical characteristic and isoefficiency curves. Even with regard to the inverter, it is possible to model the losses that occur inside it more accurately, since the objective is to obtain the electrical power supplied by the storage system. The total losses of the inverter are therefore related to the conduction and switching losses in all the devices, both in the IGBTs or MOSFETs [32], and in the freewheeling diodes. In this work, these losses were taken into account through the inverter efficiency η_{Inv}, which is usually made available by the manufacturer.

$$P_{battery} = \frac{P_{EM}}{\eta_{Inv}} \tag{5}$$

The efficiency of the inverter depends on the power supplied with respect to the rated power data of the inverter itself. The following Figure 6, purely indicative, represents the variation in efficiency with respect to the percentage of output power normalised with respect to the nominal power.
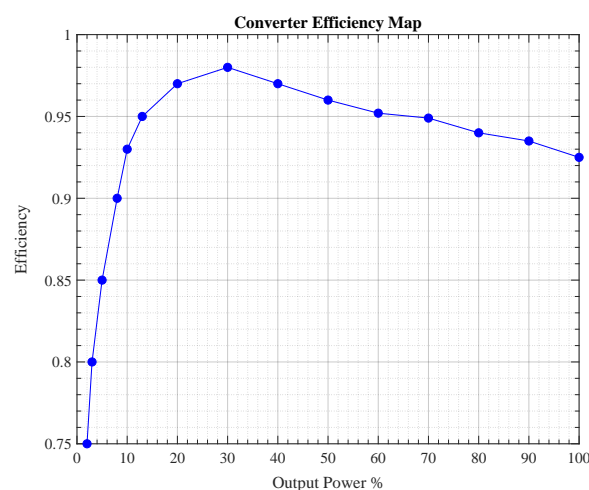

Figure 6. Converter efficiency map.

3.4. Battery Model

In the literature, there are mainly three categories of battery models, depending on the type of approach with which they are implemented and the kind of battery. These models are divided into electrochemical models, electrical circuit models, and mathematical models [33]. However, the battery models proposed for sizing the storage system for railway systems are based on the mathematical models [23,34] or equivalent circuit models [35,36].

In this work, the battery model available in MATLAB/Simulink software for a lithium-ion battery was used. This circuit model was initially proposed in [37] and later modified in [38,39]. The models proposed in [35–37] do not take into account the exponential trend of the breakdown voltage in the areas of maximum charge and discharge. Therefore, in order to improve the accuracy of the mathematical model with respect to the real dynamic behaviour of the battery, terms that take into account the exponential trend of the electrical quantities were added in this model [38,39]. The circuit in this model consists of a controlled voltage generator, which allows the open-circuit voltage of the battery and its variation as a function of the state of charge (SOC) to be modelled, and a series resistor *R*, which allows internal voltage drops to be taken into account. In order to better represent the non-linear behaviour of the open-circuit voltage, the polarisation parameter *K* was added. The battery current *i*∗ was filtered through a low-pass filter in order to avoid the algebraic loop during the simulation. The Figure 7 shows the schematic of the proposed model.
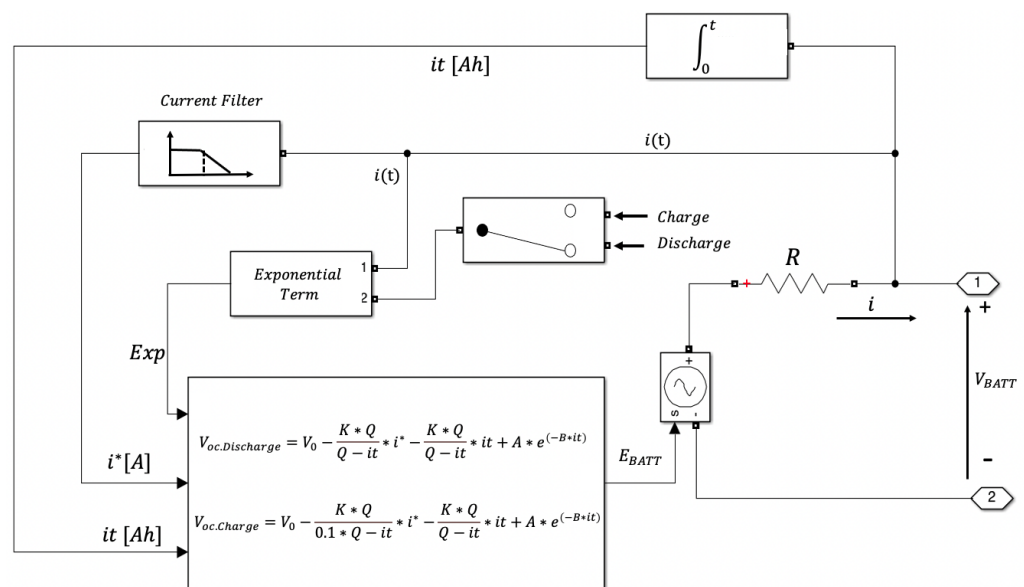

Figure 7. Schematic diagram of the battery model.

The equations representing the battery voltage and open-circuit voltage are, respectively:

$$V_{battery} = E_o - \frac{K * Q}{Q - it} i(t) - Ri(t) \tag{6}$$

$$V_{OC} = E_o - \frac{K * Q}{Q - it} * i(t) \tag{7}$$

E_o is the no-load voltage with the battery fully charged and is a constant, Q is the maximum capacity of the battery (it is the discharged capacity given by the integral of the current flowing in the battery), K is the bias constant, and R is the internal resistance. The polarisation parameter K can be expressed by the equation:

$$K = \beta V_{full} - V_{nom} + A(\exp^{-BQ_{nom}} - 1) \frac{(Q_{full} - Q_{nom})}{Q_{nom}} \tag{8}$$

V_{full} is the maximum battery voltage. V_{nom} is the nominal voltage. Q_{nom} and Q_{full} are the capacity at the nominal voltage and the capacity when the battery is fully charged. The equations describing the no-load voltage behaviour across the battery are further distinguished

when the battery is discharged or charged. For lithium-ion batteries, the following equations are used to describe the change in no-load voltage as a function of discharged capacity:

$$V_{OC_{Discharge}} = E_0 - \frac{K * Q}{Q - it} * i^* - \frac{K * Q}{Q - it} it + A \exp^{(-B * it)} \tag{9}$$

$$V_{OC_{Charge}} = E_0 - \frac{K * Q}{0.1 * Q - it} * i^* - \frac{K * Q}{Q - it} it + A \exp^{(-B * it)} \tag{10}$$

The state of charge (SOC) is estimated using the following equation:

$$SOC = 1 - \frac{1}{Q} \int_0^t i(t) * dt \tag{11}$$

In which the constant Q is the maximum capacity of the battery. For the parameters A and B, the equations are as follows:

$$A = V_{full} - V_{exp} \tag{12}$$

$$B = \frac{\alpha}{Q_{exp}} \tag{13}$$

The parameter A is given by the difference between the battery voltage at full charge and the battery voltage at the end of the exponential segment; thus, A represents the amplitude of the exponential voltage zone. B is the exponential capacitance, also called the inverse time constant. This parameter is calculated using the battery capacity at the end of the exponential segment and is related to a constant parameter α obtained by fitting the model to the actual battery data. In addition, i^* is the measured current value filtered through a first-order low-pass filter.

4. Sizing and Component Selection

4.1. Electric Motor and Inverter

The design of the entire electric drive was performed starting from the power demand of the vehicle under the worst conditions, i.e., at the maximum slope and maximum speed. Indeed, under the most-difficult conditions, the vehicle must be able to start from a standstill on the maximum slope and move at the maximum constant speed. From the dynamic model of the vehicle, the required mechanical power at constant speed can be estimated, then the appropriate motor and inverter will be dimensioned to meet the power requirements. The mechanical characteristic of the electric motor is closely related to the mechanical characteristic of the vehicle shown in Figure 8, which represents the tractive effort and, thus, the force with which the vehicle can be moved at different speeds.

The power required at the wheel when the vehicle is on a slope with a maximum gradient is obtained by imposing a ramp speed reference, which, starting from 0 Km/h, reaches an operating speed of 9 Km/h. The maximum possible acceleration of the vehicle is defined by the maximum tractive effort bounded by the grip, which depends on the adherent weight, i.e., the weight bearing on the driving wheels. In this case, having only one driven axle and choosing a coefficient of adhesion equal to 0, 18, it is possible to estimate the limit of adhesion imposed on the tractive effort as 38,808 N. The maximum resistance to motion offered by the vehicle in conditions of maximum slope at 9 Km/h is equal to 8197 N. Consequently, the power required P_d to maintain the vehicle at 9 Km/h in conditions of maximum gradient is:

$$P_d = R * v \tag{14}$$

where R is the resistance to motion calculated previously and v is the maximum speed of the vehicle. The nominal power of the electric motor is defined as the ratio of the required power to the efficiency of the mechanical transmission η_t.

$$P_{EM} = \frac{P_d}{\eta_t} = \frac{20.49 \text{ kW}}{0.95} = 21.57 \text{ kW} \tag{15}$$

The engine's maximum torque will be limited by the grip limit and is given by the following equation:

$$T_{max} = \frac{F_{max} * r}{\eta_t \tau} = 473 \text{ Nm} \tag{16}$$

The maximum torque T_{max} is given by the maximum tractive effort F_{max} and the wheel radius. The relationship between the torque at the wheel and the motor torque is given by the transmission ratio τ and the efficiency η_t. In this application, the mechanical transmission ratio was 41. The angular speed of the engine, expressed in revolutions per minute, when the vehicle is travelling at a speed of 9 Km/h is given by:

$$\omega_{EM} = \frac{v}{r} * \tau = 2094 \text{ rpm} \tag{17}$$

Therefore, an electric motor with a rated power of 25 kW was chosen. Figure 8 shows the map of the isoefficiency curves and the maximum torque curve in operation as a motor and as a generator as a function of the speed of the electric motor sized and purchased in this project.
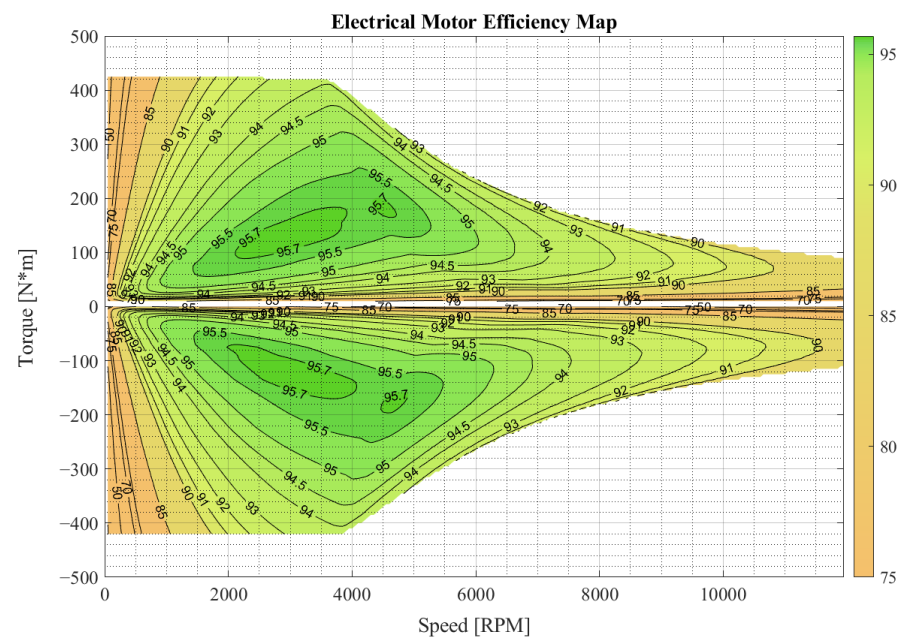

Figure 8. The mechanical characteristic and efficiency curves of the designed electric motor.

In this application, it was necessary to comply with the dimensions allowed by the approved truck already present on the vehicle structure, so the final choice of the electric motor was the result of a trade-off between the maximum torque desired for the correct operation and the bulk of the motor. In order to allow the motor to operate at high efficiency, it was necessary to use a high transmission ratio of the mechanical gearbox between the electric motor and the vehicle's wheel axle. In this way, even at low longitudinal vehicle speeds, it can be possible to work at high speed and with much lower torque. The electric motor chosen to drive the vehicle was an interior permanent magnet synchronous motor, as shown in Figure 9.

The design of the inverter was closely related to the electrical power and, consequently, the current required to power the electric motor under all expected operating conditions. In addition to the nominal electric power values, it was also necessary to consider the peak values associated with the vehicle's acceleration phases. The inverter must, therefore, be able to supply peak electrical power in addition to the nominal power. The peak electrical power is related to the peak torque, which is required to impart a certain acceleration to the vehicle. In conditions of the maximum gradient of the railway track, and therefore maximum resistance to motion, a peak torque of 179 Nm and an electric power of 40 kW are required. The calculation was based on the design requirement that the vehicle reaches a speed of 9 km/h in 9 s and, therefore, an acceleration of 0.27 m/s². The following Table 3 shows the electrical characteristics of the selected inverter. The torque control is managed by the inverter and is the MTPA vector control "maximum torque per unit of current". This type of control is excellent in the case of the interior permanent magnet synchronous motor, which is the type of electric motor that was selected.

Figure 9. The electrical motor and traction inverter.

Table 3. Parameters of the selected inverter.

Inverter Parameter	Value
Peak power	60 kW
Continuous power	35 kW
Nominal voltage	650 V
Maximum DC voltage	780 V
Full torque current available	250 V to 720 V

4.2. Choice of the Battery System

The selection of the chemical technology for the traction battery fell on lithium-ion, as this technology has countless advantages for traction applications, such as a high energy density and, thus, a low weight in relation to available energy, with the possibility of being discharged/charged at high currents [36,40,41].

The battery voltage was the DC bus voltage; therefore, no DC–DC interface converter needed to be installed between the battery and the voltage bus. The reason this was possible is due to the chemistry of the battery selected, which is in fact a lithium iron phosphate (LiFePO4) battery. This battery uses lithium iron phosphate as the cathode material and has numerous advantages, including low cost, high specific capacity, greater resistance to ageing, and above all, excellent voltage stability even when subjected to heavy loads [40]. The voltage variation at the various discharged capacitances was only a few volts, and this characteristic allowed the battery to be used without interfacing it with any voltage-stabilising converter, as shown in Section 5. In addition, the decision not to provide a DC–DC converter was also linked to the type of inverter chosen, as the converter selected has a wide range of acceptable input voltage on the DC side, which allows it to work with a variable voltage without incurring overvoltage or undervoltage conditions.

To size the storage system, it was necessary to start from the electric power necessary to feed the electric drive in the worst condition of use of the vehicle. During the sizing

phase of the motor and inverter, the mechanical power required to move the vehicle at a speed of 9 Km/h and at the maximum gradient was evaluated. From the efficiency of the electrical motor and inverter, it was possible to estimate the electric power supplied by the battery in that phase and evaluate the sizing of the storage system. The efficiency of the electric motor can be extracted from the isoefficiency curves at the operating point considered. In this case, the motor efficiency can be estimated at 0.96. As far as the inverter is concerned, the electric power required by the inverter to power the electric motor net of the losses of the latter is equal to:

$$P_{Inv} = \frac{P_{EM}}{\eta_{EM}} = \frac{21.57 \text{ kW}}{0.96} = 22.47 \text{ kW} \tag{18}$$

In this particular case, the efficiency of the inverter corresponds to approximately 0.98. It is possible to make an initial estimate of the electric power supplied by the storage system:

$$P_{battery} = \frac{P_{EM}}{\eta_{EM} * \eta_{Inv}} = \frac{21.57 \text{ kW}}{0.96 * 0.98} = 23 \text{ kW} \tag{19}$$

However, this power value represents a value absorbed under running conditions, ignoring vehicle starting. The requirement to be imposed in terms of range, which justifies the use of the vehicle, is that the battery should be able to power the vehicle for at least a 2 h work cycle. Therefore, the storage system to be sized should have an energy of 46 kWh to be able to complete the work cycle at the maximum speed and the maximum gradient in 2 h, discharging the battery from 100% to 0%. Due to the high susceptibility of lithium-ion batteries to deep discharges, which result in the loss of performance and a decrease in overall lifetime, it is necessary to avoid over-discharging the battery, so it was decided to keep a degree of discharge (DOD) of 80% and, therefore, assume that the battery is discharged from 100 to 20 of its maximum capacity. Thus, in this case, the capacity of 46 kWh was the energy discharged with a DOD of 80%, and therefore, the maximum capacity of the storage system to be selected was 57.5 kWh. The market research on storage systems focused on suppliers who already develop modules and systems used in railway applications. Traction battery systems designed for applications in this field have a number of standards and reference regulations that must be met when working in this field [42]. The battery purchased is shown in Figure 10, and its parameters are summarised in Table 4.

Figure 10. The battery system designed.

Table 4. Parameters of the selected lithium-ion battery.

Battery Parameter	Value
Nominal Voltage	665.6 V
Nominal Power	83 kW
Available Energy	56 kWh
Maximum Capacity	105 Ah
Maximum Voltage	760 V
Minimum Voltage	572 V
Nominal Current	125 A
Peak Current	200 A (60 s)

4.3. Chopper DC/DC and Braking Resistor

To dimension the DC/DC converter (braking chopper) to dissipate energy on a suitable resistor (braking resistor), in the event that it cannot be used for regenerative purposes, it was necessary to quantify the power derived during the braking phases, considered within the working cycle designed for the APLA100-E vehicle. To this end, a simulation data acquisition process was undertaken, assuming the vehicles start-up until the working speed of 9 Km/h was reached, keeping it and subsequent stopping. The results of the simulations made it possible to derive a power profile of the vehicle based on the work cycle hypothesised in the preliminary phase, the net of the times required for the start-up and stop transients, which depend on the slope conditions of the stretch on which the vehicle operates.

For the sizing of the devices, it was decided to consider the worst-case scenario, which can be identified in the hypothesis of performing the work cycle at a gradient of $-35‰$. In this condition, maintaining a working speed of 9 Km/h assumes a continuous electric braking condition, generating a power of 22 kW, and for stopping, this power had a peak of 60 kW. For the dimension of the DC/DC converter suitable for dissipating the excess electrical energy during braking on a suitable resistor, it was necessary to know the peak DC current during the braking phase. The total braking energy is derived as:

$$E_{tot} = P_{br_{peak}} * t_{br} \tag{20}$$

where t_{br} and $P_{br_{peak}}$ are the time and peak power value during braking, respectively. A factor known as the Braking Ratio (BR) is defined as the ratio of the braking time to the time of an entire work cycle, as derived from the following Equation (8).

$$BR = \frac{t_{br}}{T_{cicle}} \tag{21}$$

The nominal power output at the ends of the braking resistor is defined by Equation (9).

$$P_{br_{nom}} = P_{br_{peak}} * \frac{t_{br}}{2 * T_{cicle}} = \frac{E_{tot}}{T_{cicle}} \tag{22}$$

The braking voltage V_{br} corresponds to the DC bus voltage during the phenomenon of interest. Its value depends on the state of charge of the battery. The average and peak current during the braking phase are defined as follows:

$$I_{br_{average}} = \frac{E_{tot}}{t_{br} * V_{br}} \tag{23}$$

$$I_{br_{peak}} = \frac{P_{br_{peak}}}{V_{br}} \tag{24}$$

Once the peak current and DC bus voltage have been defined, the braking resistance can be determined using Ohm's law.

$$R_{br} = \frac{V_{br}}{I_{br_{peak}}} \tag{25}$$

The DC bus voltage value has a great influence on the dimension of the resistor. At this point, it was decided to size the system for two different operating conditions, the first relating to the braking unit being inserted in the condition of maximum battery charge, which corresponds to a voltage value on the DC bus of 728 V, which will be the intervention threshold of the converter. On the other hand, in the hypothesis of being able to command the braking unit to intervene, a worst-case condition was assumed in which the battery was deeply discharged, but could not receive charging current. In this case, the DC bus would be at a voltage level of 572 V. Table 5 summarises the calculations performed for both cases.

Table 5. Calculation of braking resistance for the two cases.

Parameters	Case 1	Case 2
Voltage	728 (V)	572 (V)
Energy	1380 (kJ)	1380 (kJ)
Peak power	60 (kW)	60 (kW)
Rated power	14.4 (kW)	14.4 (kW)
Peak current	82.417 (A)	104.9 (A)
Average current	35.766 (A)	45.52 (A)
Braking resistor	5.5 (Ω)	8.83 (Ω)

For the sizing of the braking resistor, the worst case was considered to extinguish a peak current of approximately 105 *A*, and thus, a resistor of 8.83 Ω was implemented. The choice of the braking chopper was made according to all the electrical parameters discussed, and it must in fact be able to manage the electrical power to be dissipated both in steady state conditions and in peak conditions. Obviously, the chopper must be able to operate within the battery voltage range. The following Table 6 shows the characteristics of the brake chopper that was identified.

Table 6. Parameters of the selected braking chopper.

Chopper Parameters	Value
Peak Current	100 A
Nominal Current	50 A
Max Voltage	965 V

5. Experimental Results

In order to carry out the tests, the vehicle was placed on the track at the Tesmec plant in Monopoli, Italy; the size of the track section is approximately 20 m and has a slope of 0‰. The work cycle was then created and used to perform the simulations by managing the speed setpoint at 9 Km/h and the electric braking from 9 Km/h to 0. The work cycle actually performed and the drive torque developed by the electric motor are shown in Figure 11. On the vehicle, the main network on which information travels is the CAN bus network; using this network via a CAN–USB converter, the electrical quantities of the components can be obtained. The bit rate of the CAN network is 250 kpbs. The current, voltage, and state of charge signals were acquired via current and voltage transducers, while the SOC was the result of a processing algorithm created by the battery management system. Through a resolver mounted on the axis of the electric motor, it was possible to obtain the vehicle speed by knowing the wheel radius and transmission ratio. The prototype was tested for a work cycle of forty minutes, in which the rail vehicle carried out typical railway maintenance tasks. Figure 11 shows the various speed, torque, and power profiles, and it can be seen that the sized storage system manages to meet the

required power. During the braking phase, the torque is negative, and the electric motor acts as a generator; some of the energy is recovered. On the other hand, when the vehicle is stationary, the operating machine on the vehicle is activated to perform maintenance services, and therefore, from the graph, it is clear in that section that the electric power is absorbed. The system that was designed was powered exclusively by the lithium-ion battery, which completely eliminates emissions during the working cycle of the rail vehicle. However, the emissions that would be produced by the same vehicle if it were powered entirely by the emergency diesel generator for a one-hour work cycle would be 9.6 kg CO_2. This value of emissions was calculated from the technical data provided by the manufacturer of the emergency diesel generator on board the vehicle.
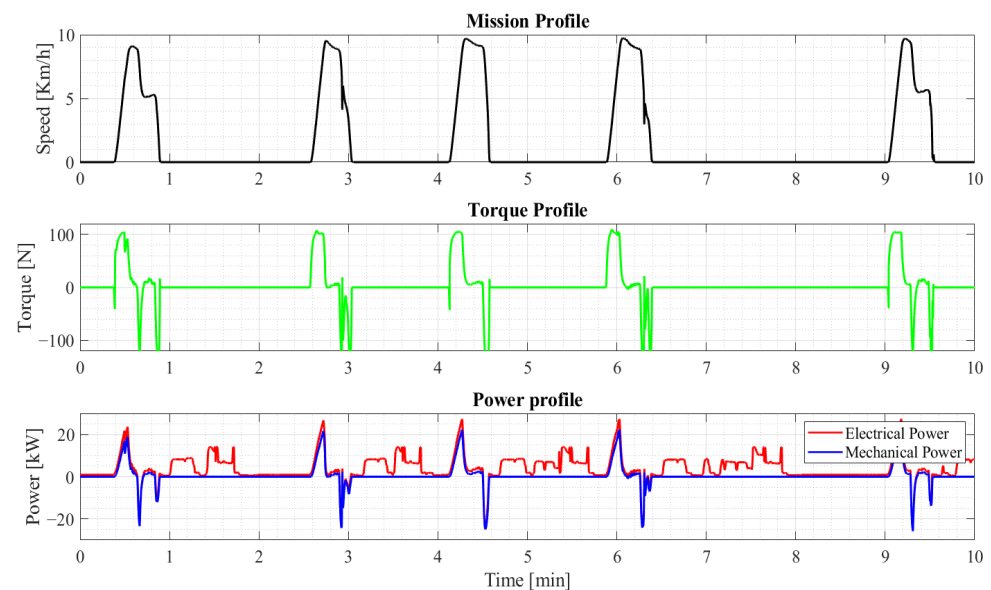
Figure 11. View of speed, torque, and power profile acquired during experimental tests.

Figure 12 compares the simulated and real energy consumption obtained during the experimental tests. The electrical energy consumption values for a 40 min work cycle were approximately 3 kWh. It can be seen that the estimated energy consumption obtained from the simulation followed the real trend accurately in the first few minutes and diverged increasingly during the work cycle; this was due to the imperfect slight inaccuracy in the modelling of the auxiliary loads, which are present throughout the operation of the vehicle.
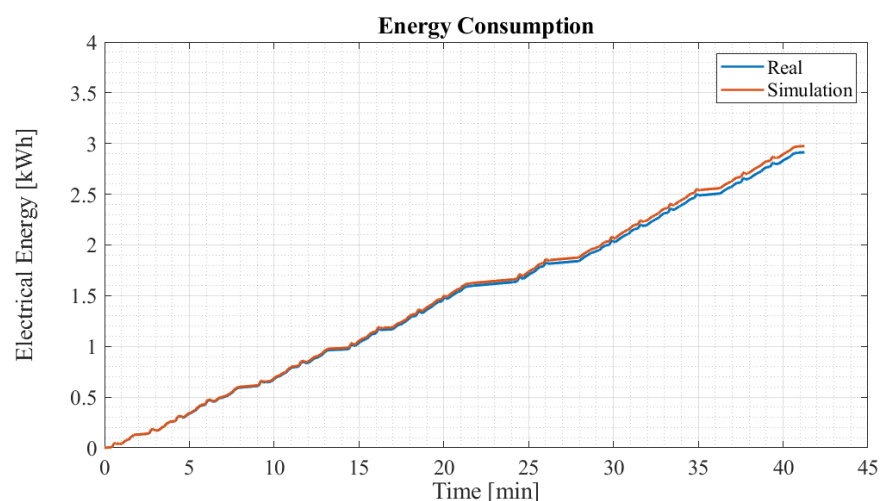
Figure 12. Simulated and real energy consumption of the railway system.

However, analysing the graphs proposed in Figure 13, the maximum absolute error and relative error were still quite low at 0.062 and 0.022, respectively. Table 7 shows other error values related to energy.
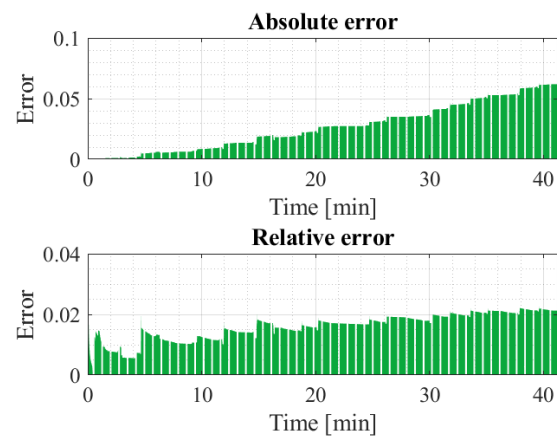

Figure 13. Representation of the variation over time of the absolute error and relative error of electrical energy consumption.

Table 7. Calculation of electrical energy consumption error.

Indicators	Electrical Energy Consumption
Mean absolute error	0.0263
Mean square error	0.001
Root-mean-squared error	0.0323
Maximum percentage error	2.2%

The efficiency of the propulsion system was calculated during the experimental tests by Equation (26); the highest value was 86.7%, and it was reached at the maximum speed of 9 Km/h, while the lowest efficiencies were at the low speed values, as shown in Figure 14.

$$\eta_{PROP} = \frac{P_{Electrical}}{P_{Mechanical}} \tag{26}$$
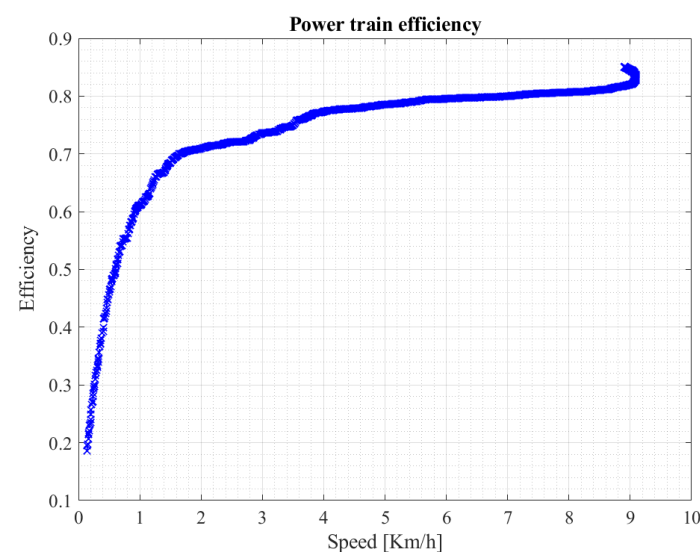
Figure 14. Profile of speed, torque, and power acquired during experimental tests.

In this work, the study and experimental tests were carried out for a prototype in which cost minimisation was not considered, but safety was primarily addressed; an example

is the implementation of the braking resistor. Therefore, an economic view in terms of investment and installation costs was not provided, but through the design procedure based on mathematical modelling, it was possible to calculate the electrical energy recovered during the braking phases of the vehicle. Indeed, considering the worst-case scenario in which the vehicle works with a gradient of 0‰ and for a working cycle of two hours, it was possible to recover about 1.77 kWh during braking, which corresponds to an energy savings of 16.5%. This is a particularly advantageous savings for countries such as Italy, where the cost of electricity is around EUR 0.5/kWh.

Once the battery was sized, it was purchased, and the proposed model was validated at steady state through the experimental data of the dynamic performance provided by the battery manufacturer. In fact, experimental tests were performed on the battery and compared with those obtained through the simulation to prove the validity of the model, as shown in Figure 15.
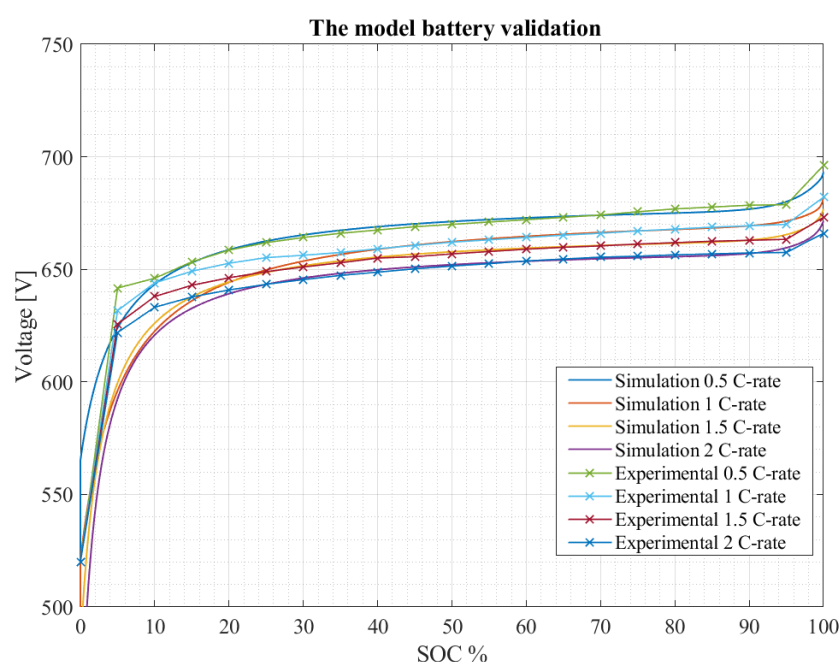
Figure 15. Comparison of the voltage–discharge curve values obtained from the model with the values carried out during the experimental tests on the battery.

It can be seen from Figure 15 how the measured voltage was lower when the battery was discharged with a higher current, but the voltage trend remained practically constant within the range, which varied between 90% of the state of charge and 20% with a decrease of only 20 V. The maximum voltage reached 696 V at 100% of the state of charge, while it suddenly dropped below 600 V once the battery was almost completely discharged (SOC between 10% and 0%).

From the state of charge that was acquired during the tests from the battery with a sampling time of 1s, a comparison between the estimated state of charge obtained in the simulation and that obtained experimentally is shown in Figure 16.

Figure 17 shows the comparison between the amplitude of the voltage and current measured during the experimental tests and those estimated using the mathematical model implemented in the simulation.
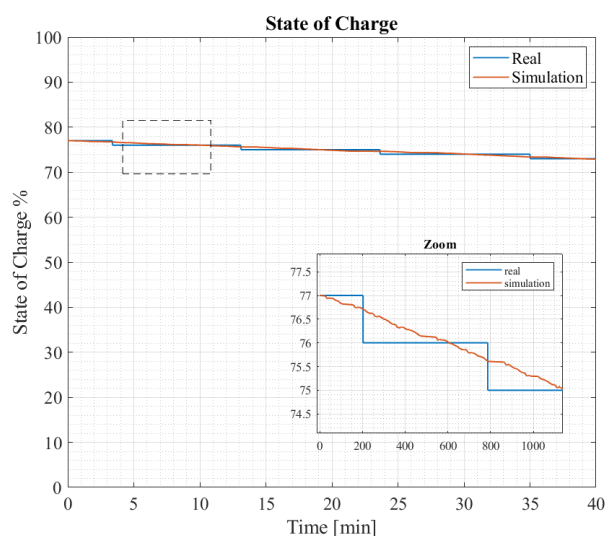
Figure 16. Comparison of the state of charge value obtained from the model and that achieved during the experimental tests.
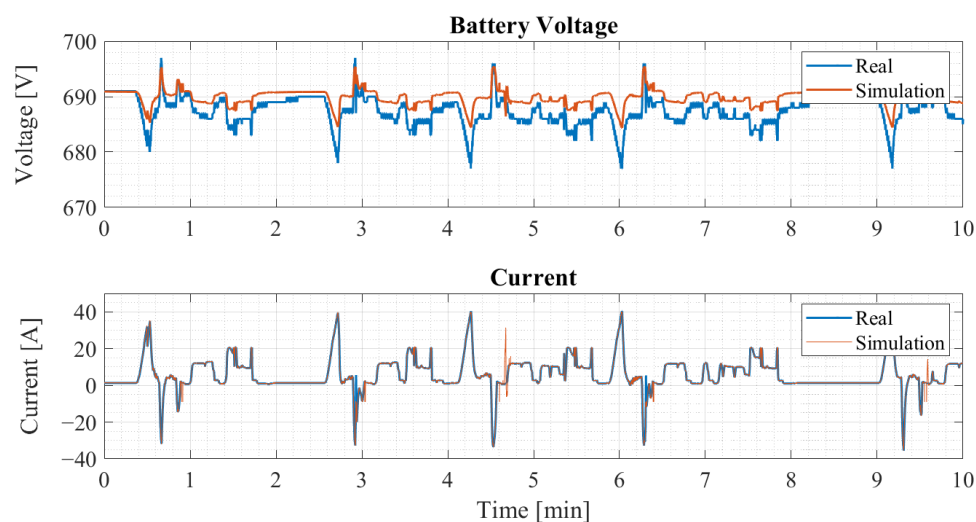

Figure 17. Representation of current and voltage amplitude during simulation and experimental test.

The waveforms of the battery voltage and the current drawn by the propulsion system were compared with the corresponding quantities measured during the experimental tests. The percentage error of the battery voltage and current were approximately 1.28% and 1%, respectively. The quantities were well estimated by the implemented model, as can also be seen from the indicators in Table 8, which validates the reliability of both the simulated results and the presented design procedure.

Table 8. Calculation of voltage and current error.

Indicators	Voltage	Current
Mean absolute error	3.0680	0.1422
Mean square error	10.99	0.9782
Root-mean-squared error	3.316	0.9891
Maximum percentage error	1.28%	1%

6. Conclusions

In this paper, the design procedure for the electrification of a railway vehicle was presented, from the analyses carried out in simulation, to the design and procurement of

the propulsion and generation components of the vehicle, through to the experimental tests on the constructed prototype. The analysis and preliminary studies for the design were carried out using simulations in the MATLAB/Simulink environment. The electrical energy consumed for a 40 min work cycle was approximately 3 kWh. The percentage error and the absolute maximum error calculated from the difference between the simulated and experimentally measured value of consumed energy were 2.2% and 0.062, respectively. The experimental tests carried out on the prototype proved the effectiveness of the design procedure adopted and the proposed mathematical model, showing a good matching with the simulated results. The lithium-ion storage system model was validated through the results of the experimental tests performed on the battery. The experimental results performed on the vehicle validated the design procedures and reliability of the entire designed propulsion system. The tests were carried out on a 20 m track on which Tesmec Rail Srl tests its vehicles. The vehicle was subjected to a real working cycle lasting 40 min, and the efficiency of the entire powertrain was 86.7% when the vehicle reached its maximum design speed.

References

1. International Energy Agency (IEA); International Union of Railways (UIC). *Railway Handbook 2017—Energy Consumption and CO₂ Emissions*; Tech. Rep. 6; IEA: Paris, France, 2017.
2. European Commission. *2020 by 2020 Europe's Climate Change Opportunity*; COM (2008) 30 Final; European Commission: Brussels, Belgium, 2008.
3. UIC; CER. Moving towards Sustainable Mobility: A Strategy for 2030 and beyond for the European Railway Sector, Paris. 2012. Available online: http://www.cer.be/sites/default/files/publication/CER-UIC_Sustainable_Mobility_Strategy_-_SUMMARY.pdf (accessed on 28 January 2021).
4. UN. Kyoto Protocol to the United Nations Framework Convention on Climate Change, Kyoto. 1998. Available online: https://unfccc.int/resource/docs/convkp/kpeng.pdf (accessed on 22 January 2021).
5. UN. Paris Agreement, Paris. 2015. Available online: https://unfccc.int/sites/default/files/english_paris_agreement.pdf (accessed on 22 January 2021).
6. Liu, Z.; Song, Y.; Han, Y.; Wang, H.; Zhang, J.; Han, Z. Advances of research on high-speed railway catenary. *J. Mod. Transport.* **2018**, *26*, 1–23. [CrossRef]
7. Bruni, S.; Bucca, G.; Carnevale, M.; Collina, A.; Facchinetti, A. Pantograph-catenary interaction: Recent achievements and future research challenges. *Int. J. Rail Transp.* **2018**, *6*, 57–82. [CrossRef]
8. Song, Y.; Zhang, M.; Øiseth, O.; Rønnquist, A. Wind deflection analysis of railway catenary under crosswind based on nonlinear finite element model and wind tunnel test. *Mech. Mach. Theory* **2022**, *168*, 104608. [CrossRef]
9. The Future of Rail. Available online: https://www.iea.org/futureofrail/ (accessed on 20 September 2019).
10. Brenna, M.; Bucci, V.; Falvo, M.C.; Foiadelli, F.; Ruvio, A.; Sulligoi, G.; Vicenzutti, A. A Review on Energy Efficiency in Three Transportation Sectors: Railways, Electrical Vehicles and Marine. *Energies* **2020**, 13, 2378. [CrossRef]
11. Siemens. Mireo Plus B Ortenau for SFBW, Baden-Württemberg, Germany. Available online: https://assets.new.siemens.com/siemens/assets/api/uuid:636c61e0-bd2d-4f97-a2c7-78e690792a44/mors-b10022-00dbmireoplusortenauenus-72_original.pdf (accessed on 16 December 2022).

12. RailwayTechnology. Bombardier Talent 3 Battery Train. Available online: https://www.railway-technology.com/projects/bombardier-talent-3-battery-train/ (accessed on 16 December 2022).
13. Ghaviha, N.; Campillo, J.; Bohlin, M.; Dahlquist, E. Review of Application of Energy Storage Devices in Railway Transportation. *Energy Procedia* **2017**, *105*, 4561–4568. [CrossRef]
14. Alstom. Alstom's Hydrogen Train Enters Regular Passenger Service in Austria. Available online: https://www.alstom.com/press-releases-news/2020/9/alstoms-hydrogen-train-enters-regular-passenger-service-austria (accessed on 16 December 2022).
15. FuelCellWorks. Siemens Mireo Plus H Fuel Cell Hydrogen Train—The Middle Distance Champion. Available online: https://fuelcellsworks.com/news/siemens-mireo-plus-h-fuel-cell-hydrogen-train-the-middle-distance-champion/ (accessed on 16 December 2022).
16. IRJ. Zillertalbahn Hydrogen Train Design Revealed. Available online: https://www.railjournal.com/fleet/zillertalbahn-hydrogen-train-design-revealed/ (accessed on 16 December 2022).
17. Alfieri, L.; Iannuzzi, D.; Mottola, F.; Pagano, M.; Roscia, M. Battery-Based Energy Storage Systems for Catenary-Free Electric Trains. In Proceedings of the 2018 IEEE International Conference on Electrical Systems for Aircraft, Railway, Ship Propulsion and Road Vehicles International Transportation Electrification Conference (ESARS-ITEC), Nottingham, UK, 7–9 November 2018; pp. 1–6.
18. Yang, Y.; Zhang, W.; Wei, S.; Wang, Z. Optimal Sizing of On-Board Energy Storage Systems and Stationary Charging Infrastructures for a Catenary-Free Tram. *Energies* **2020**, *13*, 6227. [CrossRef]
19. Mwambeleko, J.J.; Kulworawanichpong, T. Battery Electric Multiple Units to Replace Diesel Commuter Trains Serving Short and Idle Routes. *J. Energy Storage* **2017**, *11*, 7–15. [CrossRef]
20. Fragiacomo, P.; Piraino, F.; Genovese, M.; Flaccomio Nardi Dei, L.; Donati, D.; Migliarese Caputi, M.V.; Borello, D. Sizing and Performance Analysis of Hydrogen- and Battery-Based Powertrains, Integrated into a Passenger Train for a Regional Track, Located in Calabria (Italy). *Energies* **2022**, 15, 6004. [CrossRef]
21. Polater, N.; Tricoli, P. Technical Review of Traction Drive Systems for Light Railways. *Energies* **2022**, *15*, 3187. [CrossRef]
22. Nategh, S.; Boglietti, A.; Liu, Y.; Barber, D.; Brammer, R.; Lindberg, D.; Aglen, O. A Review on Different Aspects of Traction Motor Design for Railway Applications. *IEEE Trans. Ind. Appl.* **2020**, *56*, 2148–2157. [CrossRef]
23. Kapetanović, M.; Vajihi, M.; Goverde, R.M.P. Analysis of Hybrid and Plug-In Hybrid Alternative Propulsion Systems for Regional Diesel-Electric Multiple Unit Trains. *Energies* **2021**, *14*, 5920. [CrossRef]
24. Schmid, S.; Ebrahimi, K.; Pezouvanis, A.; Commerell, W. Model-based comparison of hybrid propulsion systems for railway diesel multiple units. *Int. J. Rail Transp.* **2017**, *6*, 16–37. [CrossRef]
25. Haxhiu, A.; Abdelhakim, A.; Kanerva, S.; Bogen, J. Electric Power Integration Schemes of the Hybrid Fuel Cells and Batteries-Fed Marine Vessels—An Overview. *IEEE Trans. Transp. Electrif.* **2021**, *8*, 1885–1905. [CrossRef]
26. Chacko, R.V.; Sreedevi, M.L.; Mineeshma,G.R. Electric vehicle power train simulation in forward modelling approach to enable real-time simulation and HIL controller prototyping. In Proceedings of the 2014 IEEE International Conference on Power Electronics, Drives and Energy Systems (PEDES), Mumbai, India, 16–19 December 2014; pp. 1–6. [CrossRef]
27. Horrein, L.; Bouscayrol, A.; Delarue, P.; Verhille, J.N.; Mayet, C. Forward and Backward simulations of a power propulsion system. *IFAC Proc. Vol.* **2012**, *45*, 441–446. [CrossRef]
28. Gao, D.W.; Mi, C.; Emadi, A. Modelling and Simulation of Electric and Hybrid Vehicles. *Proc. IEEE* **2007**, *95*, 729–745. [CrossRef]
29. Cole, C. Longitudinal train dynamics. In *Handbook of Railway Vehicle Dynamics*; Taylor & Francis: London, UK, 2006; pp. 239–278.
30. Wu, Q.; Spiryagin, M.; Cole C. Train energy simulation with locomotive adhesion model Rail. *Eng. Sci.* **2020**, *28*, 75–84. [CrossRef]
31. Carpignano, A. *Meccanica dei Trasporti Ferroviari e Tecnica della Locomozione*; Levrotto Bella: Torino, Italy, 1985.
32. Loncarski, J.; Monopoli, V.G.; Cascella, G.L.; Cupertino, F. SiC-MOSFET and Si-IGBT-Based dc-dc Interleaved Converters for EV Chargers: Approach for Efficiency Comparison with Minimum Switching Losses Based on Complete Parasitic Modelling. *Energies* **2020**, *13*, 4585. [CrossRef]
33. Tamilselvi,S.; Gunasundari, S.; Karuppiah, N.; Razak RK, A.; Madhusudan, S.; Nagarajan, V.M.; Sathish, T.; Shamim, M.Z.M.; Saleel, C.A.; Afzal, A. A Review on Battery Modelling Techniques. *Sustainability* **2021**, *13*, 10042.
34. de la Torre, S.; Sánchez-Racero, A.J.; Aguado, J.A.; Reyes, M.; Martínez, O. Optimal Sizing of Energy Storage for Regenerative Braking in Electric Railway Systems. *IEEE Trans. Power Syst.* **2015**, *30*, 1492–1500. [CrossRef]
35. Herrera, V.I.; Gaztañaga, H.; Milo, A.; Saez-De-Ibarra, A.; Etxeberria-Otadui, I.; Nieva, T. Optimal energy management and sizing of a battery-supercapacitor-based light rail vehicle with a multiobjective approach. *IEEE Trans. Ind. Appl.* **2016**, *52*, 3367–3377. [CrossRef]
36. Olmos, J.; Gandiaga, I.; Lopez, D.; Larrea, X.; Nieva, T.; Aizpuru, I. Li-Ion Battery-Based Hybrid Diesel-Electric Railway Vehicle: In-Depth Life Cycle Cost Analysis. *IEEE Trans. Vehic. Tech.* **2022**, *71*, 5715–5726. [CrossRef]
37. Shepherd, C.M. Design of Primary and Secondary Cells—Part 2. An equation describing battery discharge. *J. Electrochem. Soc.* **1965**, *112*, 657–664. [CrossRef]
38. Tremblay, O.; Dessaint, L.-A.; Dekkiche, A.-I. A Generic Battery Model for the Dynamic Simulation of Hybrid Electric Vehicles. In Proceedings of the 2007 IEEE Vehicle Power and Propulsion Conference, Arlington, TX, USA, 9–12 September 2007; pp. 284–289.
39. Tremblay, O.; Dessaint, L.A. Experimental Validation of a Battery Dynamic Model for EV Applications. *World Electr. Veh. J.* **2009**, *3*, 289–298. [CrossRef]

40. Turcheniuk,K.; Bondarev, D.; Amatucci, G.G.; Yushin, G. Battery materials for low-cost electric transportation. *Mater. Today* **2021**, *42*, 57–72. [CrossRef]
41. Hannan, M.A.; Hoque, M.M.; Hussain, A.; Yusof,Y.; Ker, P.J. State-of- the-art and energy management system of lithium-ion batteries in electric vehicle applications: Issues and recommendations. *IEEE Access* **2018**, *6*, 19362–19378. [CrossRef]
42. Standard IEC 62924:2017 Railway Applications—Fixed Installations—Stationary Energy Storage System for DC Traction Systems 2017. Available online: https://www.sis.se/api/document/preview/8024733/ (accessed on 16 December 2022).